PCCP

Accepted Manuscript

ROYAL SOCIETY OF CHEMISTRY

www.rsc.org/pccp

An Abnormally Slow Proton Transfer Reaction in a Simple HBO Derivative due to Ultrafast Intramolecular-Charge Transfer Events

Noemí Alarcos,[1≠] Mario Gutierrez,[1≠] Marta Liras,[2] Félix Sánchez,[2] and Abderrazzak Douhal[1*]

Abstract

We report on the steady-state, picosecond and femtosecond time-resolved studies of a charge and proton transfers dye 6-amino-2-(2'-hydroxyphenyl)benzoxazole (6A-HBO) and its methylated derivative 6-amino-2-(2'-methoxyphenyl)benzoxazole (6A-MBO), in different solvents. With femtosecond resolution and comparing with the photobehaviour of 6A-MBO, we demonstrate for 6A-HBO in solution, the photoproduction at S_1 of an intramolecular charge-transfer (ICT) process taking place in ~140 fs or shorter, followed by solvent relaxation in the charge transferred species. The generated structure (syn-enol charge transfer conformer) experiences an excited-state intramolecular proton-transfer (ESIPT) reaction to produce a keto-type tautomer. This subsequent proton motion happens in 1.2 ps (n-heptane), 14 ps (DCM) and 35 ps (MeOH). In MeOH, it is assisted by the solvent molecules and occurs through tunneling for which we got a large kinetic isotope effect (KIE) of about 13. For the 6A-DBO (deuterated sample in CD_3OD) the global proton-transfer reaction takes place in 200 ps, showing a remarkable slow KIE regime. The slow ESIPT reaction in DCM (14 ps), not through tunnelling as it not sensitive to OH/OD exchange, has however to overcome an energy barrier using intramolecular as well as solvent coordinates. The rich ESIPT dynamics of 6A-HBO in the used solutions is governed by an ICT reaction, triggered by the amino group, and it is solvent dependent. Thus, the charge injection to 6A-HBO molecular frame makes the ICT species more stable, and the phenol group less acidic, slowing down, the subsequent ESIPT reaction. Our findings bring new insights on the coupling between ICT and ESIPT reactions on the potential-energy surfaces of several barriers.

1. Introduction

Proton transfer (PT) is one of the most fundamental processes involved in chemical and biochemical reactions.[1] This process can be either intra- or intermolecular in nature, and could take place in the ground- and excited-states. The excited-state intramolecular proton transfer (ESIPT) reaction involving hydrogen atom (or proton) donor and acceptor groups within the same molecule generally takes place in very short time (<100 fs) via preformed intramolecular hydrogen bonds (IHB).[2-10] When the donor and acceptor sites do not meet the geometrical requirements for an IHB, a H-bonding solvent may play the role of a proton-relay, and the excited-state intramolecular proton transfer is then assisted by the solvent molecules. During the last three decades, excited-state proton-transfer dyes have been much studied, leading to different applications, as fluorescent chemosensors,[11, 12] laser dyes,[13-17] UV photostabilizers[18] and promising components for photoswitches,[19-22] and organic optoelectronic materials.[23-25]

The photoinduced proton-transfer reaction in organic molecules having electron-donor or –acceptor substituents in the molecular framework will be affected by a possible intramolecular charge-transfer (ICT) process making that both ESIPT and ICT reactions can occur separately (stepwise fashion) or simultaneously (synchronous way), i.e. they are coupled. In the first option, one can distinguish two mechanisms: I) a proton motion in the so-called enol form followed by a charge transfer (E→PT→ICT)[26] and II) a charge transfer in E followed by a proton motion (E→ICT→PT).[27-29] When the rates of both events are about the same, we cannot distinguish between both mechanisms and in this case the reactions are coupled (E→ICT/PT).[30] The presence or absence of barriers for both processes makes the potential-energy surfaces (PES) very rich for a possible control of the related spectroscopy and dynamics using shaped pulses or confining media.[31-35] Several theoretical works have reported on the issue of proton coupled charge transfer processes, and limits have been examined.[36, 37] From the point of view of experiments, using aromatic molecules undergoing such processes, a number of studies have been done using derivatives of 2-(2'-hydroxyphenyl)benzoxazole (HBO) and 2-(2'-hydroxyphenyl)benzothiazole (HBT) having electron acceptor substituent (-NO_2, -COOH, -COOR or -RCN) in the benzazole ring.[26, 38, 39] For these popular dyes, the proposed mechanism is a proton motion followed by a charge transfer process. These reports have suggested that the rate of the ICT process is determined mostly by

the solvent nature in which the polarity plays a key role.[26, 38, 39] Thus, the presence of an electron-acceptor group in the benzazole ring photoproduces, after of a very fast ESIPT process, an ICT process in the keto-type tautomer (K*) to give a charge transfer keto (KCT*) form. However, when the substituent is an electron donor group (-NH_2, -NR_2 or -CH_3) the ICT process occurs prior to the ESIPT one. An example of this kind of mechanism is provided by the behaviour of 2-(2'-hydroxy-4'-diethylaminophenyl)benzothiazole.[40] In this molecule, the electron-donating substituent (-$N(C_2H_5)_2$) in the phenol part, gives an electronic density to the molecule so the acidity of the hydroxyl group is significantly reduced and therefore, a lowering in the ESIPT rate constant was observed.[40] In aprotic polar solvent, the ESIPT process takes place over a barrier induced by the solvent polarity.[40] Other type of molecules that show this type of reactions is presented by the 4-N,N-dialkylamino-3-hydroxyflavone family.[29, 30, 41-43] Here a large change in the dipole moments of the normal (N*) and the tautomer (T*) forms is observed due to the presence of the N,N-dialkylamino group. As a result, the proton transfer rate constant is affected by the solvent polarization.[29] A previous study of this kind of flavones and using femtosecond resolution showed that the ultrafast ICT reaction is followed by the ESIPT process.[28] On the other hand the forward or equilibrated reactions are sensitive to the solvent nature.[44] The nature and position of the substituent in the molecular frame of the dye can modulate the forward/backward ESIPT rates ratio.[45] Thereby, we also have studied how the ESIPT reaction changes with the position of the –NH_2 group on the benzoxazole part of 5-amino-2-(2'-hydroxyphenyl)benzoxazole (5A-HBO).[46, 47]

Thus, the nature of the mechanism of coupled proton and charge transfers depends on the nature of the electron donor/acceptor substituent and its place in the molecular frame. To further explore this issue, we have recently reported on the fs-ns photobehaviour of an HBO amino derivate, 6-amino-2-(2'-hydroxyphenyl)benzoxazole (6A-HBO), in few solvents (ACN, THF, acetone and dioxane) where the ESIPT reaction takes place after the ultrafast ICT one in the excited enol form. In these solvents, we observed an equilibrium between the keto and ICT structures.[48] Here, the stepwise mechanism is different to that observed in others HBO and HBT derivatives where the ICT reaction is subsequent to the proton motion one.[26, 38, 39]

To better understand the behaviour of 6A-HBO, we studied its photodynamics in other solvents with different polarity, basicity and H-bonding ability. Thus, we report on steady-state and fs-ns studies of 6A-HBO and its methoxy derivative 6-amino-2-(2'-

methoxyphenyl)benzoxazole (6A-MBO) (Scheme 1) in n-heptane, dichloromethane (DCM) and methanol (MeOH) solutions. For 6A-MBO which cannot undergo an ESIPT reaction, due to the amino group we observed times of ICT reaction (~150 fs) together with solvent relaxation (1-5 ps) comparable to those observed in other media.[48] For 6A-HBO, in addition to the ICT process a subsequent and slow irreversible ESIPT reaction takes place in the syn-enol charge transfer (syn-ECT) species, contrary to the behaviour in other solvents where the proton motion is reversible.[48] Furthermore, the ESIPT reaction time is strongly dependent on the solvent nature: while in n-heptane, the keto type structure is formed in ~1.2 ps, in DCM solution it is slower (14 ps). In MeOH solution, it is also slower and takes place via tunneling in 35 ps, while it occurs in 200 ps (abnormally large KIE around 13) for the 6A-DBO in CD_3OD. Our results clearly give new findings in coupled intramolecular charge and proton transfer reactions dynamics in a simple derivative of a widely studied proton-transfer dye.

2. Experimental

Details of the synthesis, purification and characterization of 6-amino-2-(2'-methoxyphenyl)benzoxazole (6A-MBO), 6-amino-2-(2'-hydroxyphenyl)benzoxazole (6A-HBO) and 6-amino-2-(2-hydroxyphenyl)benzoxazole-d_3 (6A-DBO) are described in the ESI†. Briefly the synthesis of the benzoxazoles was carried out following the steps described in Scheme S1 (ESI†). First of all, we synthesized the nitro amines HBAN and MBAN compounds by condensation between 2-amino-5-nitrophenol and the corresponding 2-substituted benzaldehyde. Afterward, we made the cyclization to the corresponding nitrobenzoxazol 6NO_2-HBO and 6NO_2-MBO using two different methods depending of the presence of hydroxyl or methoxy groups. A quantitative reduction of these new dyes with H_2-Pd/C lead to 6-amino-2-(2'-methoxyphenyl)benzoxazole (6A-MBO) and 6-amino-2-(2'-hydroxyphenyl)benzoxazole (6A-HBO). On the other hand, the deuterated compound (6A-DBO) was obtained by reaction of 6A-HBO with deuterated methanol and evaporation.

For the spectroscopic studies, the solvents (anhydrous): n-heptane (99%), dichloromethane (DCM, 99.9%) and methanol (MeOH, 99.8%) were purchased all from Sigma-Aldrich and were used as received. The solvents (deuterated): dichloromethane

(DCM-d_2, 99.9%) and methanol- d_4 (CD_3OD, 99.8%) were purchased from Sigma-Aldrich and Scharlau, respectively and were used as received. For the pKa measurements, deionized water, hydrochloric acid solution containing 33% of HCl (Scharlau), and sodium hydroxide (Scharlau, 100%) were used to prepare aqueous solutions of different pH values.

The steady-state UV-visible absorption and fluorescence spectra have been recorded using JASCO V-670 and FluoroMax-4 (Jobin-Yvone) spectrophotometers, respectively. Fluorescence quantum yield of 6A-MBO and 6A-HBO in used solvents were measured using Quinine Sulfate in 0.1 N H_2SO_4 solution, as a reference ($\varphi = 0.51$ at 293 K).[49]

Picosecond emission decays were measured by a time-correlated single photon counting (TSCPC) system.[50] The sample was excited by a 40-ps pulsed diode laser centred at 371nm (<5 mW, 40 MHz repetition rate). The emission signal was collected at the magic angle and the instrument response function (IRF) was ~70 ps. The decays were deconvoluted and fitted to a multiexponential function using the FLUOFIT package (PicoQuant) allowing single and global fits. The quality of the fit was estimated by χ^2, which was always below 1.1. The time-resolved emission spectra (TRES) were constructed from the single-wavelength measurement, and the zero time spectrum was taken as the one obtained at the intensity half-maximum corresponding to the rise of the excitation pulse.

The femtosecond (fs) emission transients have been collected using the fluorescence up-conversion technique. The system consists of a femtosecond Ti:sapphire oscillator (MaiTai HP, Spectra Physics) coupled to a second harmonic generation and up-conversion setups.[51] The oscillator pulses (90 fs, 250 mW, 80 MHz) were centred at 700 nm and doubled in an optical setup through a 0.5-mm BBO crystal to generate a pumping beam at 350 nm (~ 0.1 nJ). The polarization of the latter was set to magic angle in respect to the fundamental beam. The sample has been placed in a 1-mm thick rotating cell. The fluorescence was focused with reflective optics into a 1.0-mm BBO crystal and gated with the remaining fundamental fs-beam. The IRF of the full setup (measured as a Raman signal of pure solvent) was 220 fs. To analyse the decays, a multiexponential function convoluted with the IRF was used to fit the experimental transients. Using this procedure, we can resolve components of ~50 fs. All the experiments were performed at 293 K.

3. Results and Discussion

3.1. Steady-State UV-visible Absorption and Fluorescence Spectra

To begin with, we studied the steady-state spectral behaviour 6A-MBO and 6A-HBO (Scheme 1) in n-heptane, DCM, and MeOH solutions. Figure 1 shows the corresponding steady-state UV-visible absorption and emission spectra of (~10^{-6} M) diluted solutions. The $S_0 \rightarrow S_1$ absorption spectra of 6A-MBO, in the three solvents show a unique band without any vibrational structure, and whose maxima are located at 327, 330 and 334 nm for n-heptane, DCM and MeOH solutions, respectively. The maxima are slightly shifted to longer wavelengths upon increasing the solvent polarity. This band corresponds to the $S_0(\pi) \rightarrow S_1(\pi^*)$ transition of 6A-MBO ($\varepsilon_{DCM(330nm)}$= 2±0.2 x 10^4 M^{-1} cm^{-1}). In contrast, 6A-HBO absorption spectra in n-heptane and DCM solutions show the $S_0(\pi) \rightarrow S_1(\pi^*)$ transition at 337 and 340 nm, respectively, with a clear vibrational structure. An energy difference between the first two main peaks (337 and 354 nm) of 1425 cm^{-1} for n-heptane is possibly due to δ (in-plane) vibrational O-H, N-H and C-H modes, as it has been suggested in a FTIR, Raman and theoretical study of HBO derivative having NH_2 group in the phenol part.[52] Note for both solvents the shift to lower energies of the $S_0 \rightarrow S_1$ transition due to the effect of the IHB (Table 1). However, in MeOH solution, while the $S_0 \rightarrow S_1$ absorption band shows a slightly red-shifted (340 nm), its vibrational structure is lost due to specific interactions (H-bonds) between the dye and the solvent molecules. To get information on the stoichiometry of the related complexes with MeOH molecules, we recorded the absorption spectra of 6A-HBO in n-heptane solution containing different amounts of MeOH. Figure S1 (ESI†) shows the related spectra. We used the Benesi-Hildebrand model[53] to analyse the absorption intensity change at 370 nm where we observed an increase in the intensity with methanol content. The analysis gives a 1:1 stoichiometry of 6A-HBO/MeOH complexes with an equilibrium constant K_{eq}=1.4±0.2 M^{-1} at 293 K. Clearly the complex is not robust, and the effect of the involved intermolecular H-bonds is not large at the S_0 state. Scheme 1 shows a proposal for the complex in the used n-heptane:MeOH mixture. Our suggestion is based on the ps-data of the H/D isotope effect given and discussed in part 3.2.

The extinction absorption coefficient of 6A-HBO in DCM at 340 nm ($\varepsilon_{340\ nm}$= 6.8±0.3 x 10^4 $M^{-1}cm^{-1}$) is higher than the one of HBO ($\varepsilon_{333\ nm}$= 3.4±0.1 x $10^3 M^{-1}$ cm^{-1}).

This reflects the effect of the amino group on the strength of the transient absorption dipole moment in 6A-HBO. This result was observed for other molecules having amino groups in their structures.[40, 54] Moreover, the increase of ε value for 6A-HBO when compared to 6A-MBO is a result of a larger electronic configuration due to the IHB within the former.

The fluorescence spectra of 6A-MBO present large changes with the solvent nature (Figure 1A). They show a red-shift upon increasing the solvent polarity. The intensity maxima are at 385, 415 and 450 nm for n-heptane, DCM and MeOH solutions, respectively. The spectral shift is due to a photoinduced intramolecular charge-transfer (ICT) reaction in the dye, for which the charge-transfer state is more stabilized in polar solvents, as we observed in other media.[48] The spectrum in n-heptane presents an abnormal Stokes-shift which indicates that even in this non-polar solvent an ICT process occurs. The Stokes shift observed suggests the ICT reaction is due to the amino group injecting a charge into the benzoxazole part as it happens in many aromatic molecules having this electron-donating substituent.[40, 41, 44, 48, 54] We will analyse this reaction in the time-resolved emission part (3.2 and 3.3).

The emission spectra of 6A-HBO display two bands: a weak one located at the blue region and a more intense one at the red-shifted part of the spectrum. We anticipate (based on the 6A-MBO behaviour) that the blue band is due species having experienced ICT reactions, while the red-shifted one is due to tautomers (keto species) produced by ESIPT events. The blue band almost coincides with the one discussed above for 6A-MBO. The intensity maxima are at 390 nm for n-heptane, 420 nm for DCM and 450 nm for MeOH, showing the same behaviour with the solvent polarity like that of 6A-MBO. However, the red-shifted band, which appears at 500 nm for n-heptane, 485 nm for DCM and at 470 nm for MeOH, behaves in a different way to that assigned for the ICT species, experiencing a blue-shift in the emission maxima when the solvent polarity increases. To get details on the solvent ability which influences the emission spectral positions, we analysed the correlation between Kamlet-Abboud-Taft solvent parameters (α: H-bond donating ability (acidity), β: H-bond accepting ability (basicity) and π*: polarity/polarizability),[55] and the wavenumber ($\bar{\upsilon}_{em}$) of the intensity emission maxima. For the ICT band of 6A-MBO in different solvents (n-heptane, DCM and MeOH, obtained here, and ACN, THF, acetone and dioxane, taken from our previous work),[48] we obtained:

$$\bar{\upsilon}_{em}\,(cm^{-1}) = 26126 - 913\,\alpha - 2602\,\beta - 2258\,\pi^* \qquad (1)$$

(N=7, R=0.912, standard deviation (S.D.) = 609)

For the red-shifted emission band (K) of 6A-HBO, we got:

$$\bar{\upsilon}_{em}\,(cm^{-1}) = 20000 + 883\,\alpha + 19\,\beta + 661\,\pi^* \qquad (2)$$

(N=7, R=0.898, S.D. = 257)

Thus, from the analysis we conclude that for 6A-MBO (blue band, ICT species), an increase in the acidity, and especially in the basicity and polarity, produces a red-shift in the emission spectral position, whereas for 6A-HBO (red band, K species), the increase of these parameters (especially the acidity) causes the opposite effect as shown by the sign of the solvent parameters contributions. Note that the solvent basicity (β) contribution is almost 3-4 % that of the acidity (α) and of the polarity/polarizability (π*) ones, showing that its effect is not important in the spectral shift, contrary to the behavior of the ICT band in 6A-MBO. The Stokes-shift ($\Delta\nu_{ss}$) for the red band is also solvent dependent, and has a value between 8000 and 9600 cm^{-1} (Table 1). Figure S2 (ESI†) gives another presentation of the absorption and emission spectra of both compounds in the same solvents, where we can clearly see the solvent effect on the spectra of the same dye. Note the change of $\Delta\nu_{ss}$ for 6A-MBO with the solvent nature.

The global fluorescence quantum yield of 6A-HBO has values of 0.04±0.005, 0.06±0.007 and 0.11±0.01 for n-heptane, DCM and MeOH solutions, respectively, while those of 6A-MBO in the same solvents are higher: 0.54±0.02, 0.65±0.03 and 0.72±0.03 (Table 1). This large change was also observed for 2-(2'-R-4'-diehtylaminophenyl)benzothiazole, where the quantum yield value changes from 0.85 to 0.006 in cyclohexane when R is methoxy or hydroxyl group, respectively.[40] We measured the pK_a of their neutral and protonated species in water solutions at the ground and excited states (Figures S3 and S4, ESI†), and compared the latter with those of known HBO to get the amino group effect on the electronic density at the proton donor (OH) and acceptor (-N=) sites. At S_0, the pK_a ($-NH^+=$ of the benzoxazole ring) in 6A-MBO is 3.47±0.2, very similar to the obtained for 6A-HBO, whose pK_a ($-NH^+=$ of the benzoxazole ring, and the phenol -OH part of 6A-HBO) values are 3.45±0.12 and 10.11±0.15, respectively. At S_1, the pK_a* values for 6A-HBO are 5.02±0.09 ($-NH^+=$ of the benzoxazole ring) and 2.45±0.11 (the phenol -OH part of 6A-HBO), respectively. The values at the first electronically excited-state suggest that an ESIPT reaction will take place between the benzoxazole and the phenol moieties of 6A-HBO. Thus, for 6A-

HBO in n-heptane, DCM and MeOH solutions, while the blue emission band is due to enol species having experienced an ICT process, as it happened in 6A-MBO, the longer wavelength emission one is due to a keto-type tautomer as result of an ESIPT reaction. This is in agreement with previous studies of HBO[10, 56] where it was observed a band at 500 nm assigned to the keto tautomer. The pK_a values of HBO (phenol and protonated benzoxazole parts) at S_0 are $pK_a(OH) = 10.4$[57]; $pK_a(-NH^+=) = -0.3$[57], and at S_1 are $pK_a^*(OH) = -0.04$[57], 1.35[58] (we measured 0.5), and $pK_a(-NH^+=) = 5.24$[57]. The effect of the amino group on the acidity/basicity of the benzoxazole part is clear at S_0, as it increments its basicity by ΔpK_a (pK_a(6A-HBO) - pK_a(HBO)) = 3.8, reflecting an increase the electronic density of the nitrogen site at S_0 and thus a charge transfer of the amino group. That at S_1 does not experience much change which suggests an electronic redistribution in favour of other sites. For the phenol moiety, the variation at S_0 is very week (-0.3) for the pK_a. However, at S_1 it is large: 2, making a lower acidity in the 6A-HBO phenol moiety when compared to the one in HBO parent compound. The above data point to a large electronic redistribution in 6A-HBO at S_1, making a difference in the spectroscopy and dynamics of HBO and 6A-HBO in solution, in agreement with we have observed in the steady-state emission spectra. We will examine the interplay of these changes in the related ICT/ESIPT dynamics.

The fluorescence excitation spectra of 6A-MBO and 6A-HBO in n-heptane, DCM and MeOH (Figures S5 and S6, respectively, ESI†) solutions show bands very similar to the obtained in the absorption ones. The excitation spectra of 6A-HBO in n-heptane and DCM show vibrational structures, while in MeOH this structure is not observed due to 6A-HBO:MeOH complexes formation described above. Based on these results, the observed steady-state emission bands are mainly due to species photogenerated from single structures at S_0 (syn-enol form, Scheme 1). The time-resolved experiments will give more information.

3.2. Picosecond Time-Resolved Fluorescence Study

To get information on ICT, ESIPT and non-radiative processes, we examined the ps-photodynamics of both dyes in solution. Figure 2A and Figure S7A (ESI†) show representative emission decays of 6A-MBO observed at 475 nm, and upon excitation at 371 nm. Table S1 (ESI†) gives the obtained time constants (τ_i), the pre-exponential factors (a_i) and relative contributions (c_i) normalized to 100 after a monoexponential fit.

The fluorescence decay in n-heptane, DCM and MeOH gives a time constant of 1.65, 2.3 and 2.9 ns, respectively (Table S1, ESI†). We assign this component to the ICT form in similar way to the observed one in other solvents.[48] As said above, 6A-MBO shows a photoinduced ICT reaction triggered by the amino group through the benzoxazole to the phenyl part. The change in the pK_a values reflects such charge migration. The lifetime as well as the fluorescence quantum yield of this species (Table 1) increase with the solvent polarity, which indicates a decrease in the non-radiative rate constants in more polar solvents (k_{nr} (10^8 s^{-1}) = 2.7, 1.5, 1.0 in n-heptane, DCM and MeOH, respectively).

We focus now on the photodynamics of 6A-HBO in the same solvents. Figure 2 (B and C) and Figure S7 (B and C) (ESI†) display representative emission decays of 6A-HBO recorded at 395 and 550 nm. Table 2 and S2 (ESI†) give the obtained values of the time constants (τ_i), the pre-exponential factors (a_i) and relative contributions (c_i) normalized to 100 after multiexponential fits. For n-heptane solution, the lifetimes are 420 ps and 1.5 ns. The 420-ps component increases its contribution towards longer wavelengths (34-100 %). The 1.5-ns one has its maximum contribution at 395 nm, and it disappears from 475 nm. In DCM and MeOH solutions, a bi-exponential fit was used with time constants of 14 and 35 ps, and other longer ones of 600 and 615 ps, respectively (Table 2 and S2 in ESI†). Moreover, in DCM we observed an additional component of 1.7 ns, which has a weak and decreasing contribution (~16-6%) in the signal, when observing between 395-425 nm. This component completely vanishes from 450 nm (Table 2 and S2 in ESI†). Remark that, the shortest component (14 and 35 ps) is decaying at the blue part of the spectrum, and rising at the red one, which indicates a common process occurring in the excited 6A-HBO in DCM and MeOH solutions. The other component (600 and 615 ps) appears as decay at all the observation wavelengths, and its maximum contribution is at the red part of the spectrum (Table 2 and S2 in ESI†).

In n-heptane solution, we assign the 1.5-ns component, which has its maximum contribution at the blue side of the emission spectra, to the lifetime of the open charge-transferred enol form (open-ECT) (Scheme 1) comparable to that obtained for its methylated derivative (1.65 ns), where the ESIPT reaction does not occur. This is in agreement with the time-resolved emission spectra (TRES) (Figure 3A) where at longer delay times (2 ns) the band of the open-ECT is clearly detected. This time constant also is observed in DCM solution, so the open-ECT conformer is also present in this solvent.

The 420-ps component for n-heptane sample appears also in DCM and MeOH ones with a value of 600 and 615 ps, respectively. We assigned this component to the emission lifetime of the keto form. This specie is photoproduced as a result of an ESIPT reaction in the initially excited syn-enol form. The ESIPT reaction in n-heptane occurs below the ps-resolution of the setup (≈10 ps), while in DCM and MeOH solutions it takes place in 14 and 35 ps, respectively. Usually ESIPT reaction for this type of molecules (HBO, HBT) has short time constants of less than ~150 fs. [3, 4, 59-61] However, in this case the existence of the amino group in the benzoxazole ring provokes changes in the proton-transfer dynamics as we observed in the reversible ESIPT reaction taking place in ACN, THF, acetone and dioxane.[48] On the contrary to those observations, here we do not observe equilibrium in the proton motion. This is reflected by the relative amplitudes of the rising and decaying components at the red part ($A_2/A_1 \neq -1$; Table S2 in ESI†) of the emission spectrum. Further support to an equilibrated process is given by the time resolved emission spectra (TRES) which clearly show the disappearance of the CT emission band over time, while that of the PT one remains (Figure 3). Note that the very weak emission band at 400-420 nm is due to the open-ECT structure as said above. Interestingly, in our previous report the relative amplitudes of the rising and decaying components at the red part of the emission spectra were $A_2/A_1 = -1$, and the CT emission band in the TRES did not vanish, indicating the equilibrated ESIPT in those media. We believe that 6A-HBO keto-type tautomer does not undergo a significant twisting motion which may lead to its rotamer, in clear contrast with its analogues HBO[10, 56] and HPMO.[59] We suggest that the involvement of the ICT reaction (Scheme 2) bringing an electronic charge to the phenol part does not allow such rotation, as the C-C bond connecting both moieties will acquire a double bond character. This is reflected by the lower difference observed in the non-radiative constants (from 2.3 in n-heptane to 1.5×10^9 s^{-1} in MeOH solution). High level theoretical calculations (at S_1) or time-resolved IR experiments should give direct information to explore this suggestion.[62-64] DCM, an aprotic polar solvent will stabilize the ECT form making higher the energy barrier to cross to the keto form well (Scheme 2A), and therefore the time constant for ESIPT process is longer, 14 ps. Solvent polarity effect on the ESIPT reaction has been observed in 2-(2'-hydroxy-4'-diehtylaminophenyl)benzothiazole[40] and 4-dimethylaminoflavonol (DMAF) in agreement with our results.[28, 44] To get a spectral picture in the time domain, Figure 3B shows TRES of 6A-HBO in DCM at different gating times. The normalized (at the

intensity maximum) spectra clearly indicate the conversion of the 420-nm emission band (ECT) to the 500-nm one (K). As 6A-DBO (where OH has been changes to OD) in deuterated DCM gives similar decay and rise times (14 ps) we conclude that in DCM the ESIPT reaction does not proceed by tunneling (Figure S8, ESI†). Thus, in this solvent the proton (deuterium) motion has to overcome an energy barrier in which the degree of stabilization of ICT species prior to the keto form is solvent polarity dependent. Thus, the potential-energy surface (PES) should contain proton-transfer coordinates which involved IHB and N—OH distances, as well as an ICT one where the solvent nature plays a key role on the related dynamics.

Finally, in MeOH solution we observed a large kinetic isotopic effect (KIE) in the emission decays (Figure 4 and Table 2 and S2 in ESI†). The time constant for the proton-transfer reaction is 35 ps for 6A-HBO in MeOH but 200 ps for 6A-DBO in CD_3OD. Table 2 and S2 (ESI†) show the decays data of 6A-DBO in CD_3OD using a three-exponential function, with a short lifetime of 200 ps, an intermediate of 780 ps, and longest one of 2.4 ns. The 200-ps component appears as decay at the blue part of the spectrum, and as a rise at the red one. It is worth to note the long time constant obtained in MeOH (35 ps) and CD_3OD (200 ps) which leads us to believe that the ESIPT reaction here is assisted by the solvent. For a MeOH/n-heptane mixture, this complex is of 1:1 (6A-HBO/MeOH) nature. In neat MeOH, it might involve more alcohol molecules (i.e. interaction with $–NH_2$ group) (Scheme 1), making slower and via a proton-relay the ESIPT reaction of 6A-HBO. The large KIE (k_{OH}/k_{OD}= 13.3) indicates tunneling and the involvement of more than one MeOH molecule in the process making slower the global proton-transfer dynamics (Scheme 2B). However, for a MeOH/n-heptane mixture containing 0.7 M of MeOH (CD_3OD), we got the same rise times as in neat MeOH and CD_3OD leading us to believe that the proton relay in the ESIPT reaction involved this solvents mixture as well as in the bulk MeOH makes use of one alcohol solvent molecule at least when exciting at 371 nm. 7-hydroxyquinoline (a bifunctional molecule giving and receiving protons) in MeOH and CD_3OD showed also a large KIE explained by tunneling and slower alcohol molecules (1:2 complexes) rearrangement, where a step-wise mechanism of the protons motions was proposed.[65] Figure 3C and S9 (ESI†) show the TRES of 6A-HBO and 6A-DBO in MeOH and CD_3OD, respectively, where we can clearly see the band of ECT (~430 nm) leads to the proton (deuterium) transfer one (470 nm). The spectra of both samples reflect similar results. On the other hand, the two components observed for 6A-DBO in CD_3OD (780

ps and 2.4 ns) which appear as decays in the whole spectrum (410-500 nm), are assigned to the keto (K) and to the open-ECT forms, respectively. This behaviour is due to the slow proton motion that occurs in CD_3OD, leading to a stabilization of the open-ECT species and a longer emission lifetime. The steady-state emission spectrum reflects this difference, where the band of open-ECT is clearer for 6A-DBO in CD_3OD than for 6A-HBO in MeOH (Figure S9A, ESI†). Moreover, the TRES of 6A-DBO in CD_3OD at longer time decays (3-7 ns) show a blue-shift in the emission spectrum which is a clear indication of the open-ECT form fluorescence (Figure S9B, ESI†).

3.3. Femtosecond Time-Resolved Fluorescence

To investigate the ultrafast dynamics, we studied the femtosecond emission behaviour of both dyes in the above solvents. Exciting at 350 nm, we bring the molecular system to almost without excess of vibrational energy at S_1. Figures 5 y 6 show the fluorescence transients at the gated emission wavelengths for both dyes in solutions. Tables 3-4 and S3-S4 (ESI†) give the results of the multiexponential fits, taking into account the ps-results discussed above.

First, we focus on the ultrafast dynamics of 6A-MBO (Figure 5) as it does not undergo any proton-transfer reaction, while interrogating that of ICT one. The times for the ns-components are fixed in the fits using the values from the ps-ns experiments. For simplicity, the analysis of the transients for n-heptane and DCM solutions is divided in two different regions: region I for observation wavelengths lower than 430 nm; and region II for wavelengths longer than 420 nm. For region I, we observed a rising component of ~150 fs, and a decaying one of ~1 ps. While in region II, n-heptane sample does not show any fs-ps component, in DCM we recorded a rising component of 1.1 ps from 420 nm. Note also that the emission band in n-heptane sample is not enough large to interrogate further region. For MeOH solution, region I (370-410 nm) shows two decays with values of 280 fs and 2-3.9 ps, respectively. In region II (420-550 nm), we only observed a rising component of 0.6-5.5 ps.

In n-heptane and DCM solutions, the ultrafast rising component of ~150 fs in region I is real as it appears at the higher energy part of the emission spectrum. Figures 7A and 7B show the observed rise in a zoomed presentation. However, the blue transient in MeOH (Figure 7C) exhibits a very fast rising which is under the resolution of the system (<80 fs). We assigned the ultrafast fs-rising component (in the three

solvents) to an ICT reaction triggered by the amino group into the molecular frame of 6A-MBO (Scheme 3). The short time indicates a barrierless process. In n-heptane, despite being a nonpolar solvent, the ICT reaction can happen. Previous studies of HBO with electron withdrawing groups showed also an ICT process in a cyclohexane solution.[38, 39] Our assignment is also supported by the abnormal Stokes-shift emission spectra of 6A-MBO (4610 cm^{-1} in n-heptane, 6025 cm^{-1} in DCM and 7900 cm^{-1} in MeOH, Table 1) and also with our previous study.[48] The decaying 280-fs component in MeOH solution at 370 and 380 nm is suggested due to intramolecular vibrational-energy redistribution (IVR) and ultrafast solvent response induced by H-bonds with MeOH molecules.

The 1-ps (decay) component observed in region I for n-heptane is a mixture of: IVR and vibrational relaxation/cooling (VR/cooling). This is in agreement with previous results obtained for molecules of comparable size.[62, 66, 67] Note that this time is not observed from 430 nm indicating that it is not related to any reaction. However, we believe that the 1-ps (DCM) and up to 5-ps (MeOH) rising components at region II reflect solvation dynamics in the formed ICT species leading to a large Stoke-shift of the emission band (Figure 1, Scheme 3). As expected, the time constant corresponding to this process is longer (up to 5.5 ps) in a more polar solvent (MeOH). It is worth to note that this time is similar to the characteristic mean solvation times of MeOH (5 ps) and DCM (0.56 ps) using Coumarin 153.[68]

Now, we focus our efforts on 6A-HBO ultrafast dynamics. The results (Figures 6, and S10 in ESI†, and Tables 4 and S4 in ESI†) show decaying and rising components at the blue and red regions of the emission spectra, respectively. All the transients have an additional (few hundreds) ps-component due to the keto-type emission lifetime. Dealing with the ultrafast events here, and following the behaviour of the short components, we divided the transients in two or three regions depending on the used solvent. To begin with n-heptane solution, region I corresponds to the transients observed at 395-420 nm, while region II reflects those of 430-450 nm, and region III is when gating from 475 to 600 nm. For DCM and MeOH solutions, we distinguish only region I (up to 420 nm) and region II (430-600 nm). For n-heptane and DCM solutions, in region I we got a rising component of ~140 fs and a decaying one of 1-1.2 ps. This latter component also appears as a decay in region II in the transients of n-heptane sample, but as a rise in those of DCM ones. However it is a rise in region III for n-heptane sample. The 140-fs component, as in 6A-MBO which cannot undergo any

proton-transfer reaction, is due to ICT from the amino group to the HBO skeleton, leading to ECT species. In n-heptane, the subsequent produced keto (K) tautomer should be generated from syn-ECT in a short time (1.2 ps). Note that for 6A-MBO in n-heptane solution, we did not observe any ps-rising component at the reddest part, supporting the suggestion that the 1.2 ps rising time in 6A-HBO emission is mainly due to ESIPT reaction in the excited syn-ECT forms. However, solvation dynamics contribution of ECT species, and keto structures should happen in a similar time and they cannot be discarded in the observed transients.

In DCM solution, in addition to the ICT (140 fs) and solvation dynamics (~ 1 ps) discussed above for its methylated derivative, we observed a 14-ps decaying (regions I) and rising (region II) component (Table 4 and S4 in ESI†). The photoproduced syn-ECT structures in DCM undergo an ESIPT process in 14 ps to give the keto tautomer (Scheme 2A) as we described in the picosecond part. We observed no OH/OD isotope effect on the dynamics of ESIPT reaction in ECT (Figure S8, ESI†) suggesting a multi-dimensionality of the proton-transfer reaction and absence of tunneling. To overcome the barrier to K well, the systems should evolve along IHB and distance between the heteroatoms exchanging the proton, and possibly dihedral angle between both aromatic parts as well as solvent (polarization) coordinates of the PES. The ICT reaction brings a charge to the phenol ring making the OH group less acidic and then slower the ESIPT reaction. The charge transfer and proton motion make rich the PES of 6A-HBO to explore from the point of view of theory and wavepacket coherent control.

Finally, for MeOH solution at 380 nm, we observed non-resolved fs-rise (<100 fs) (as for 6A-MBO) and 250 fs decay in addition to 2.1 and 35 ps decays at region I, and rise at region II. As we suggested for 6A-MBO, the non-resolved fs-component in MeOH is due to ICT, while the 250 fs decay might be due to IVR and ultrafast solvent response. The 0.8-2.1-ps component is due to solvent relaxation around the initially formed ECT structures to give more stabilized ones.

To summarize this part, for 6A-HBO in solution, an ultrafast (~140 fs or shorter) ICT leads to ECT structures having a charge moved from the amino group to the HBO parts. These species will be stabilized by the solvent, and the syn-ECT ones will further experience a proton-transfer reaction in 1.2 ps (n-heptane), 14 ps (DCM) and 35 ps (MeOH) (Scheme 2). While our experimental observation using the methoxy derivative and isotope effect clearly support our mechanism of coupled ICT and ESIPT reaction in

6AHBO, high level calculations at S_1 will provide more insight into the barrier energy, electron flow and reaction coordinates. We are working in these directions.

4. Conclusions

In this work, we reported on the steady-state UV-visible absorption and emission spectra, and photodynamics of 6A-MBO and 6A-HBO in n-heptane, DCM and MeOH solutions. For 6A-MBO, we only observed one fluorescence lifetime in each solvent (1.65 ns in n-heptane, 2.3 ns in DCM and 2.9 ns in MeOH) which is assigned to the intramolecular charge transfer (ICT) structure. The fluorescence quantum yield and non-radiative rate constant are sensitive to the nature (polarity) of the solvent in agreement with the occurrence of an ICT reaction. The femtosecond experiments indicate an ultrafast ICT reaction taking place between the aniline substituent and the HBO part in ~140 fs for n-heptane and DCM and < 100 fs in MeOH solutions. The ICT event is followed by a solvent relaxation in 1 ps (n-heptane and DCM) and 5 ps (MeOH). Both ICT and solvation dynamics lead to a large Stokes shifted emission band.

For 6A-HBO in the same solvents, we observed a dual emission assigned to ICT and ESIPT structures. The emission lifetime of the keto-type structure is in the 420-615 ps range. From the point of view ps-dynamics, we also observed 14 and 35 ps decaying (blue part) and rising (red-shifted part) components for DCM and MeOH solutions, respectively, which we assign to the ESIPT reaction time. In n-heptane, the reaction occurs in 1.2 ps. In the three used solvents, the proton-transfer reaction is remarkably slow when compared to the one in the parent molecule (HBO, <150 fs). The isotopic effect (OH/OD in 6A-HBO) does not show any change in the whole dynamics for n-heptane and DCM solutions, while in CD_3OD we got a large KIE (about 13). The keto-type formation time changes from 35 ps in MeOH to 200 ps in CD_3OD. For DCM solution, we suggest that the ESIPT reaction does not occur via tunneling to bring the molecular ICT form to the keto-type one. It rather involves other intramolecular coordinates (beside the IHB one) and solvent polarization. In MeOH, the proton-transfer reaction is surprisingly assisted by the solvent, and it occurs by tunneling. With fs-resolution, we found that the ICT reaction happens in 140 fs (n-heptane, DCM) or shorter (< 100 fs, in MeOH), while solvent relaxation occurs in 1-2 ps. The stability of the syn-ECT structures makes slower the ESIPT reaction, also reflecting a large

electronic redistribution at S_1 leading to a decrease in the acidity of the phenol part when compared with that in HBO parent molecule.

Acknowledgments

This work was supported by the MINECO through projects: Consolider Ingenio 2010 (CSD2009-0050, MULTICAT), and MAT2011-25472. M.G. thanks the MINECO for the Ph.D. Fellowship.

Notes and references

[1]Departamento de Química Física, Facultad de Ciencias Ambientales y Bioquímica, and INAMOL, Universidad de Castilla-La Mancha, Avenida Carlos III, S.N., 45071 Toledo, Spain.

[2] Instituto de Química Orgánica General, IQOG-CSIC, Juan de la Cierva, 3, 28006 Madrid, Spain.

[≠]Equal contributions

*Corresponding author at Universidad de Castilla-La Mancha. Tel.: +34 925 265717; E-mail address: abderrazzak.douhal@uclm.es

Electronic Suplementary Information (ESI†) available: Figure S1 shows UV-visible absorption in n-heptane and in presence of different concentration of MeOH. Figure S2 exhibits UV-visible absorption and emission spectra of (A) 6A-MBO and (B) 6A-HBO in different solutions. Figures S3 and S4 present UV-visible absorption and emission spectra of (A) 6A-MBO and (B) 6A-HBO in different pH solutions. Figures S5 and S6 show the excitation fluorescence and absorption spectra of 6A-MBO and 6A-HBO in different solvent, respectively. Figure S7 exhibits the magic-angle emission decays of 6A-MBO and 6A-HBO in different solvent. Figure S8 shows the magic-angle emission decays of 6A-HBO and its deuterated 6A-DBO in n-heptane and DCM-d_2 solutions. Figure S9A presents the UV-visible absorption and fluorescence spectra of 6A-HBO and 6A-DBO in MeOH and CD_3OD solutions and Figure S9B displays the magic-angle time-resolved emission spectra of 6A-DBO in CD_3OD solutions. Figure S10 is for the magic-angle fs-emission transients of 6A-HBO in DCM and MeOH solutions. Figures S11-S16 give the ^1H (A) and ^{13}C (B) NMR spectra of different molecules in DMSO-d6**.** Tables S1-S4 show the values of the emission decays of 6A-MBO and 6A-HBO in

different solutions. Scheme S1 presents the synthesis of the 6A-MBO and 6A-HBO. See

DOI:

1. J. T. K. Hynes, J. P.; Limbach, H. -H.; Limbach, R. L. (eds), ed., *Hydrogen-Transfer Reactions*, 1 st vol: I-IV edn., Wiley-VCH Weinheim, Germany, 2007.
2. J. L. Herek, S. Pedersen, L. Bañares and A. H. Zewail, *J. Chem.Phys.*, 1992, **97**, 9046-9061.
3. C. Chudoba, E. Riedle, M. Pfeiffer and T. Elsaesser, *Chem. Phys. Lett.*, 1996, **263**, 622-628.
4. A. Douhal, F. Lahmani and A. H. Zewail, *Chem. Phys.*, 1996, **207**, 477-498.
5. C. Lu, R.-M. R. Hsieh, I. R. Lee and P.-Y. Cheng, *Chem. Phys. Lett.*, 1999, **310**, 103-110.
6. S. Lochbrunner, A. J. Wurzer and E. Riedle, *J. Phys. Chem. A*, 2003, **107**, 10580-10590.
7. M. Ziolek, J. Kubicki, A. Maciejewski, R. Naskrecki and A. Grabowska, *Phys. Chem. Chem. Phys.*, 2004, **6**, 4682-4689.
8. A. Douhal, M. Sanz and L. Tormo, *Proc. Natl. Acad. Sci. U.S.A.*, 2005, **102**, 18807-18812.
9. S.-Y. Park and D.-J. Jang, *J. Am. Chem. Soc.*, 2009, **132**, 297-302.
10. N. Alarcos, B. Cohen and A. Douhal, *J. Phys. Chem. C*, 2014, **118**, 19431-19443.
11. J. Wu, W. Liu, J. Ge, H. Zhang and P. Wang, *Chem. Soc. Rev.*, 2011, **40**, 3483-3495.
12. J. Zhao, S. Ji, Y. Chen, H. Guo and P. Yang, *Phys. Chem. Chem. Phys.*, 2012, **14**, 8803-8817.
13. A. Costela, J. M. Muñoz, A. Douhal, J. M. Figuera and A. U. Acuña, *Appl. Phys. B*, 1989, **49**, 545-552.
14. R. Sastre and A. Costela, *Adv. Mater.*, 1995, **7**, 198-202.
15. A. Costela, I. Garcia-Moreno, J. Figuera, F. Amat-Guerri and R. Sastre, *Appl. Phys. Lett.*, 1996, **68**, 593-595.
16. E. Martin, R. Weigand and A. Pardo, *J. Lumin.*, 1996, **68**, 157-164.
17. G. Jones, W. R. Jackson, C. Y. Choi and W. R. Bergmark, *J. Phys. Chem.*, 1985, **89**, 294-300.
18. A. P. Fluegge, F. Waiblinger, M. Stein, J. Keck, H. E. A. Kramer, P. Fischer, M. G. Wood, A. D. DeBellis, R. Ravichandran and D. Leppard, *J. Phys. Chem. A*, 2007, **111**, 9733-9744.
19. L. Lapinski, M. J. Nowak, J. Nowacki, M. F. Rode and A. L. Sobolewski, *ChemPhysChem*, 2009, **10**, 2290-2295.
20. S.-J. Lim, J. Seo and S. Y. Park, *J. Am. Chem. Soc.*, 2006, **128**, 14542-14547.
21. T. Mutai, H. Tomoda, T. Ohkawa, Y. Yabe and K. Araki, *Angew. Chem. Int. Ed.*, 2008, **47**, 9522-9524.
22. M. Sliwa, S. Letard, I. Malfant, M. Nierlich, P. G. Lacroix, T. Asahi, H. Masuhara, P. Yu and K. Nakatani, *Chem. Mater.*, 2005, **17**, 4727-4735.
23. J. E. Kwon and S. Y. Park, *Adv. Mater.*, 2011, **23**, 3615-3642.
24. S. Park, J. Seo, S. H. Kim and S. Y. Park, *Adv. Funct. Mater.*, 2008, **18**, 726-731.

25. S. Park, J. E. Kwon, S. H. Kim, J. Seo, K. Chung, S.-Y. Park, D.-J. Jang, B. M. Medina, J. Gierschner and S. Y. Park, *J. Am. Chem. Soc.*, 2009, **131**, 14043-14049.
26. J. Seo, S. Kim and S. Y. Park, *J. Am. Chem. Soc.*, 2004, **126**, 11154-11155.
27. W. Frey, F. Laermer and T. Elsaesser, *J. Phys. Chem.*, 1991, **95**, 10391-10395.
28. A. Douhal, M. Sanz, M. A. Carranza, J. A. Organero and L. Santos, *Chem. Phys. Lett.*, 2004, **394**, 54-60.
29. Y.-M. Cheng, S.-C. Pu, Y.-C. Yu, P.-T. Chou, Huang, C.-T. Chen, T.-H. Li and W.-P. Hu, *J. Phys. Chem. A*, 2005, **109**, 11696-11706.
30. P.-T. Chou, Huang, S.-C. Pu, Y.-M. Cheng, Y.-H. Liu, Y. Wang and C.-T. Chen, *J. Phys. Chem. A*, 2004, **108**, 6452-6454.
31. H. Naundorf, J. A. Organero, A. Douhal and O. Kühn, *J. Chem.Phys.*, 1999, **110**, 11286-11293.
32. M. Korolkov, J. Manz and G. Paramonov, *Chem. Phys.*, 1997, **217**, 341-374.
33. V. S. Batista and P. Brumer, *Phys. Rev. Lett.*, 2002, **89**, 143201.
34. A. Douhal, *Science*, 1997, **276**, 221-222.
35. A. Douhal, *Chem. Rev.*, 2004, **104**, 1955-1976.
36. R. I. Cukier and D. G. Nocera, *Annu. Rev. Phys. Chem.*, 1998, **49**, 337-369.
37. S. Hammes-Schiffer and A. A. Stuchebrukhov, *Chem. Rev.*, 2010, **110**, 6939-6960.
38. C.-C. Hsieh, Y.-M. Cheng, C.-J. Hsu, K.-Y. Chen and P.-T. Chou, *J. Phys. Chem. A*, 2008, **112**, 8323-8332.
39. C. H. Kim, J. Park, J. Seo, S. Y. Park and T. Joo, *J. Phys. Chem. A*, 2010, **114**, 5618-5629.
40. Y.-M. Cheng, S.-C. Pu, C.-J. Hsu, C.-H. Lai and P.-T. Chou, *ChemPhysChem*, 2006, **7**, 1372-1381.
41. S. Ameer-Beg, S. M. Ormson, X. Poteau, R. G. Brown, P. Foggi, L. Bussotti and F. V. R. Neuwahl, *J. Phys. Chem. A*, 2004, **108**, 6938-6943.
42. F. Parsapour and D. F. Kelley, *J. Phys. Chem.*, 1996, **100**, 2791-2798.
43. V. V. Shynkar, Y. Mély, G. Duportail, E. Piémont, A. S. Klymchenko and A. P. Demchenko, *J. Phys. Chem. A*, 2003, **107**, 9522-9529.
44. A. D. Roshal, J. A. Organero and A. Douhal, *Chem. Phys. Lett.*, 2003, **379**, 53-59.
45. W. Yang and X. Chen, *Phys. Chem. Chem. Phys.*, 2014, **16**, 4242-4250.
46. N. Alarcos, M. Gutiérrez, M. Liras, F. Sánchez and A. Douhal, *Photochem. Photobiol. Sci.*, 2015, **Submitted**.
47. A. Douhal, et al., to be published.
48. M. Gutierrez, N. Alarcos, M. Liras, F. Sánchez and A. Douhal, *J. Phys. Chem. B*, 2015, **119**, 552-562.
49. R. A. Velapoldi and K. D. Mielenz, *Appl. Opt.*, 1981, **20**, 1718-1718.
50. J. A. Organero, L. Tormo and A. Douhal, *Chem. Phys. Lett.*, 2002, **363**, 409-414.
51. M. Gil and A. Douhal, *Chem. Phys. Lett.*, 2006, **432**, 106-109.
52. R. M. Alves, F. S. Rodembusch, C. Habis and E. C. Moreira, *Mater. Chem. Phys.*, 2014, **148**, 833-840.
53. H. A. Benesi and J. H. Hildebrand, *J. Am. Chem. Soc.*, 1949, **71**, 2703-2707.
54. F. S. Rodembusch, F. P. Leusin, L. F. Campo and V. Stefani, *J. Lumin.*, 2007, **126**, 728-734.
55. M. J. Kamlet, J. L. M. Abboud, M. H. Abraham and R. W. Taft, *J. Org. Chem.*, 1983, **48**, 2877-2887.

56. O. K. Abou-Zied, R. Jimenez, E. H. Z. Thompson, D. P. Millar and F. E. Romesberg, *J. Phys. Chem. A*, 2002, **106**, 3665-3672.
57. M. Krishnamurthy and S. K. Dogra, *J. Photochem.*, 1986, **32**, 235-242.
58. E. L. Roberts, J. Dey and I. M. Warner, *J. Phys. Chem.*, 1996, **100**, 19681-19686.
59. D. P. Zhong, A. Douhal and A. H. Zewail, *Proc. Natl. Acad. Sci. U.S.A.*, 2000, **97**, 14056-14061.
60. M. A. Rios and M. C. Rios, *J. Phys. Chem.*, 1995, **99**, 12456-12460.
61. H. Wang, H. Zhang, O. K. Abou-Zied, C. Yu, F. E. Romesberg and M. Glasbeek, *Chem. Phys. Lett.*, 2003, **367**, 599-608.
62. T. Elsaesser and W. Kaiser, *Chem. Phys. Lett.*, 1986, **128**, 231-237.
63. P. Wnuk, G. Burdzinski, M. Sliwa, M. Kijak, A. Grabowska, J. Sepiol and J. Kubicki, *Phys. Chem. Chem. Phys.*, 2014, **16**, 2542-2552.
64. A. Sobolewski and W. Domcke, in *Ultrafast Hydrogen Bonding Dynamics and Proton Transfer Prosesses in the Condensed Phase*, eds. T. Elsaesser and H. Bakker, Springer Netherlands, 2002, vol. 23, pp. 93-118.
65. O.-H. Kwon, Y.-S. Lee, B. K. Yoo and D.-J. Jang, *Angew. Chem. Int. Ed.*, 2006, **45**, 415-419.
66. N. P. Ernsting, S. A. Kovalenko, T. Senyushkina, J. Saam and V. Farztdinov, *J. Phys. Chem. A*, 2001, **105**, 3443-3453.
67. A. Pigliucci, G. Duvanel, L. M. L. Daku and E. Vauthey, *J. Phys. Chem. A*, 2007, **111**, 6135-6145.
68. M. L. Horng, J. A. Gardecki, A. Papazyan and M. Maroncelli, *J. Phys. Chem.*, 1995, **99**, 17311-17337.

Caption of figures, schemes and tables.

Scheme 1. Possible molecular structures of 6A-MBO, 6A-HBO and 6A-HBO:MeOH complex.

Scheme 2. Proposed mechanism of 6A-HBO photodynamics at S_1 in (A) n-heptane and DCM, and (B) MeOH. The arrows indicate the nature of the photoreaction. See text for detail.

Scheme 3. Proposed relaxation dynamics of 6A-MBO from its local excited (LE) state at S_1 as a function of solvent polarity. See text for detail.

Table 1. Values of the wavelengths corresponding to the absorption and emission intensity maxima (λ), Stokes shift ($\Delta\nu_{ss}$), full width at half maximum (FWHM) of the fluorescence band intensity and global quantum yield (φ) of 6A-MBO and 6A-HBO in the used solvents.

Table 2. Values of time constants (τ_i), normalized (to 100) pre-exponential factors (a_i) and fractional contributions ($c_i = \tau_i a_i$) obtained from the fit of the emission ps-ns decays of 6A-HBO in different solutions upon excitation at 371 nm and observation as indicated. The negative sign for a_1 (c_1) indicates a rising component in the emission signal.

Table 3. Values of time constants (τ_i) and normalized (to 100) pre-exponential factors (a_i) of the functions used in fitting the fs-emission transients of 6A-MBO in different solutions, upon excitation at 350 nm and observation as indicated. (*) Fixed value in the fit taken from the TCSPC experiments (Table S1, ESI†).

Table 4. Values of time constants (τ_i) and normalized (to 100) pre-exponential factors (a_i) of the functions used in fitting the fs-emission transients of 6A-HBO in different solutions, upon excitation at 350 nm and observation as indicated. (*) Fixed value in the fit taken as a mean lifetime from the TCSPC experiments (τ_3 and τ_4 components in Table 2). The negative sign for $a_{1/2}$ ($c_{1/2}$) indicates a rising component in the emission signal.

Figure 1. Normalized to the maximum intensity uv-visible absorption and fluorescence spectra of (dashed line) 6A-MBO and (solid line) 6A-HBO in (A) n-heptane, (B)

dichloromethane (DCM), and (C) methanol (MeOH) solutions. For emission the excited wavelength was 330 nm.

Figure 2. Magic-angle emission decays of (A) 6A-MBO and, (B) and (C) 6A-HBO in (1) n-heptane, (2) DCM, and (3) MeOH solutions. The wavelength of observation is indicated as inset. The samples were excited at 371 nm. The solid lines are from the best-fit using a multiexponential function.

Figure 3. Normalized (to the maximum of intensity) magic-angle time-resolved emission spectra (TRES) of 6A-HBO in (A) n-heptane, (B) DCM and (C) MeOH gated at the indicated delay times after excitation at 371 nm. The inset gives the gating time of the spectra.

Figure 4. Representative magic-angle emission decays of (1) 6A-HBO in MeOH and (2) 6A-DBO in CD_3OD. The samples were excited at 371 nm, observed at (A) 410 nm and (B) 550 nm. The solid lines are from the best-fit a using multiexponential function.

Figure 5. Representative fs-emission transients of 6A-MBO in (A) n-heptane, (B) DCM, and (C) MeOH solutions. The samples were excited at 350 nm and the wavelength values of observation are indicated in the figure. The solid lines are from the best multiexponential fits.

Figure 6. Representative fs-emission transients of 6A-HBO in (A) n-heptane, (B) DCM, and (C) MeOH solutions. The samples were excited at 350 nm and the wavelength values of observation are indicated in the figure. The solid lines are from the best multiexponential fits.

Figure 7. Magic-angle fs-emission transients (in a short time window to see the rising fs-component) of (1) 6A-MBO and (2) 6A-HBO in (A) n-heptane, (B) DCM and (C) MeOH solutions. The samples were observed at 380 nm and excited at 350 nm. The solid lines are from the best multiexponential fits. The IRF is the instrumental response function (240 fs).

Scheme 1.

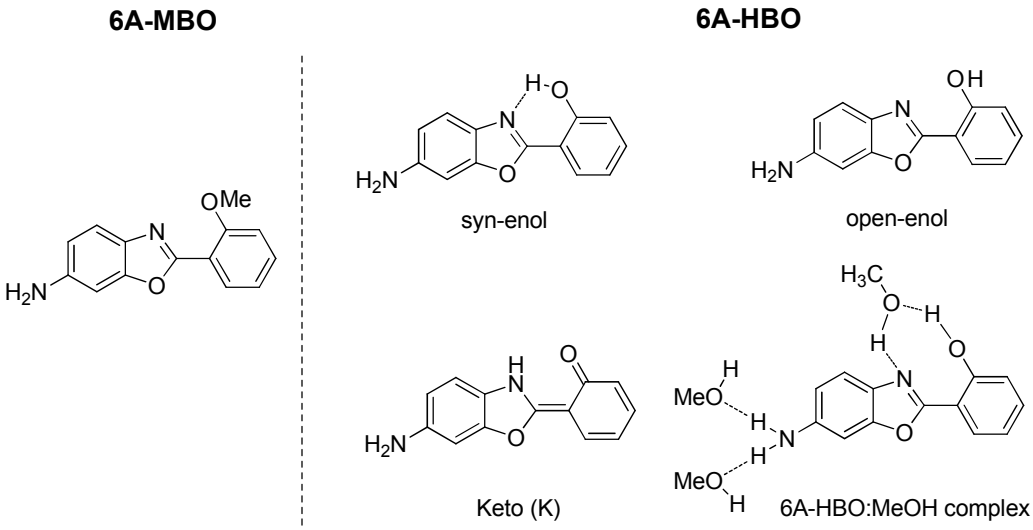

Scheme 2.

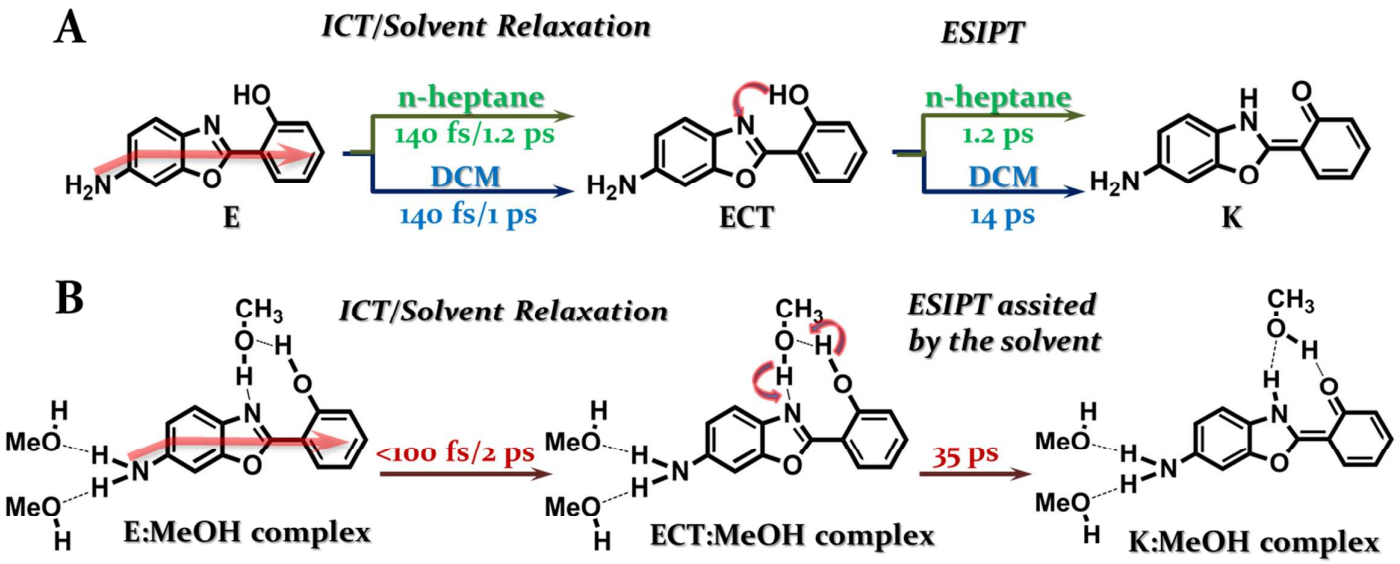

Scheme 3.

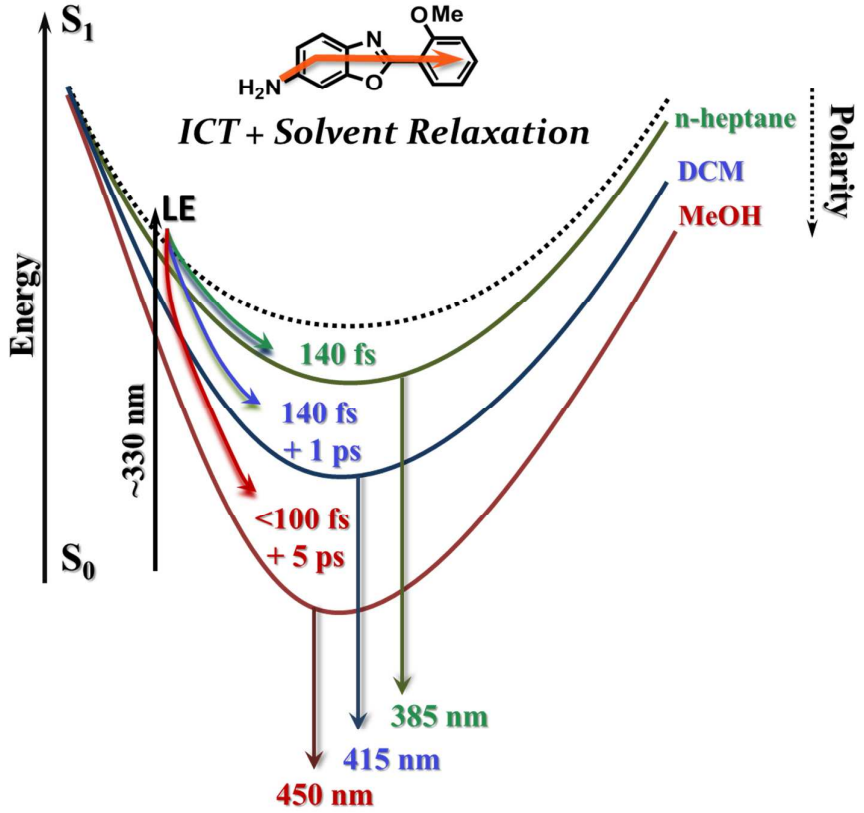

Figure 1.

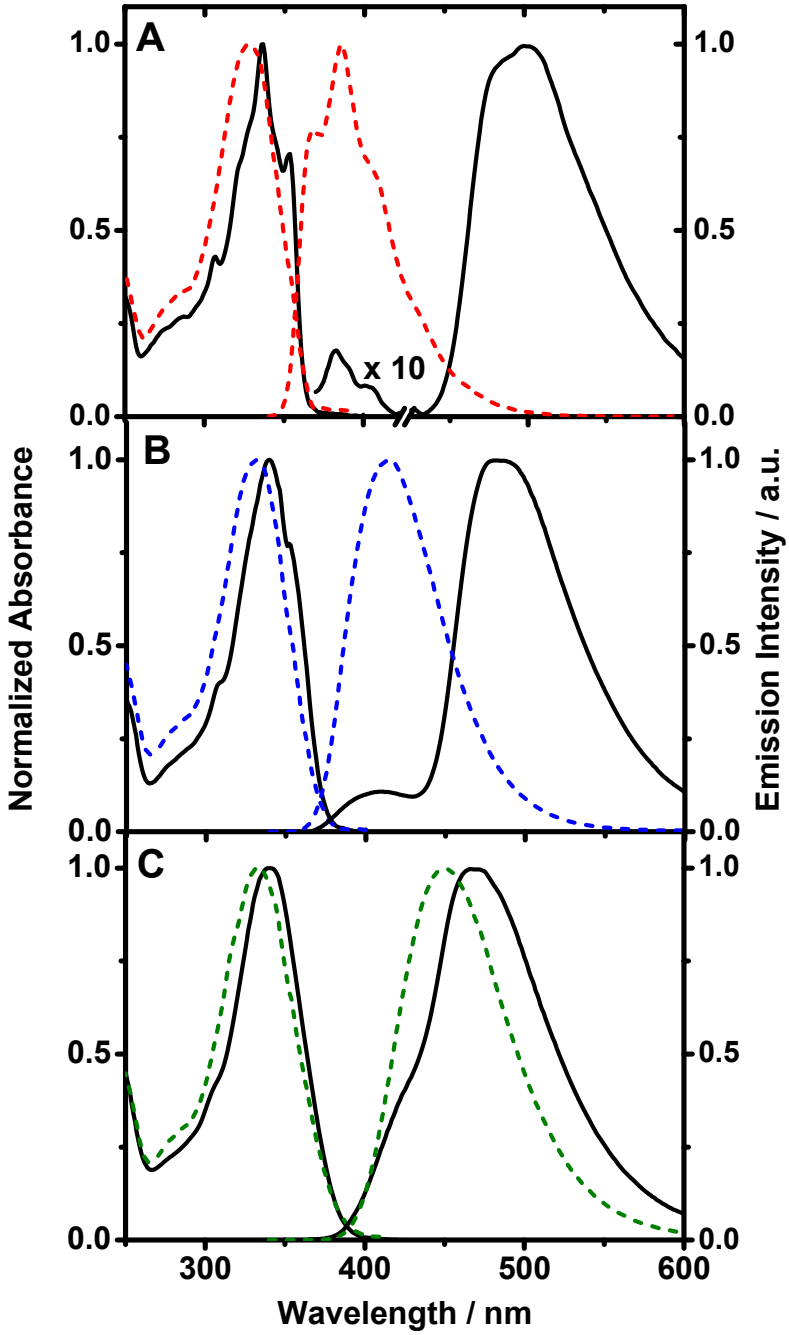

Figure 2.

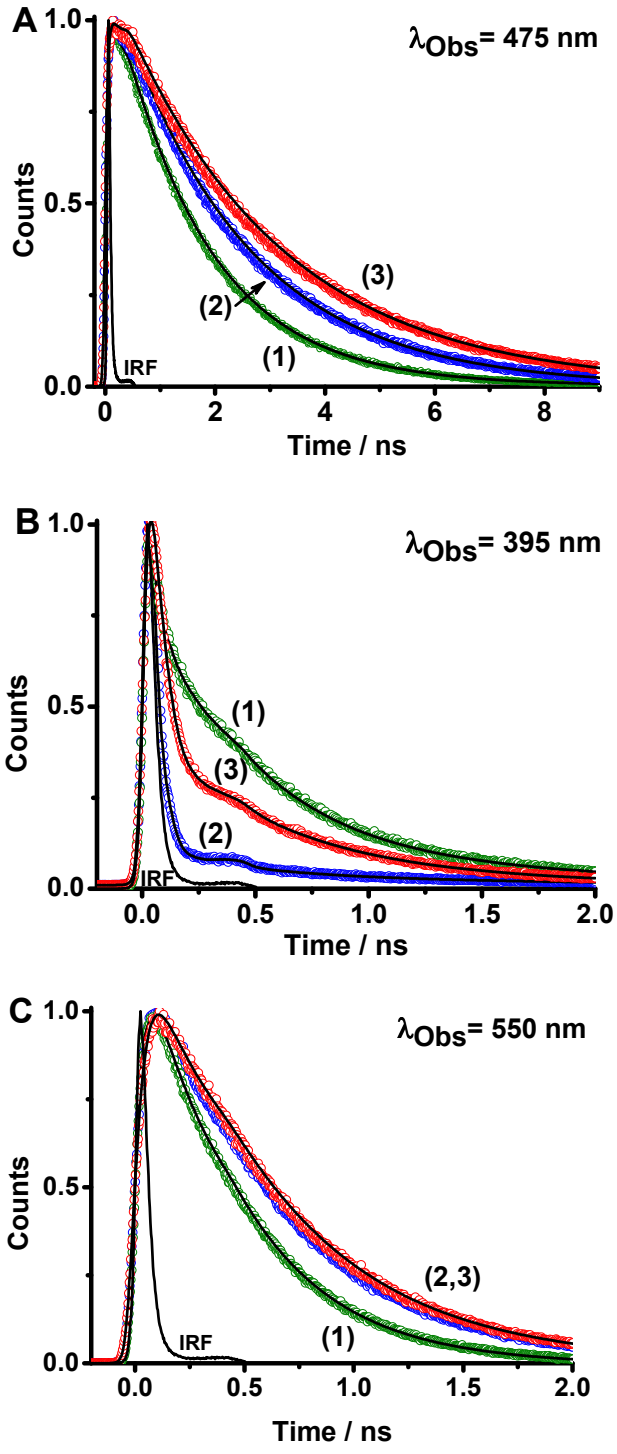

Figure 3.

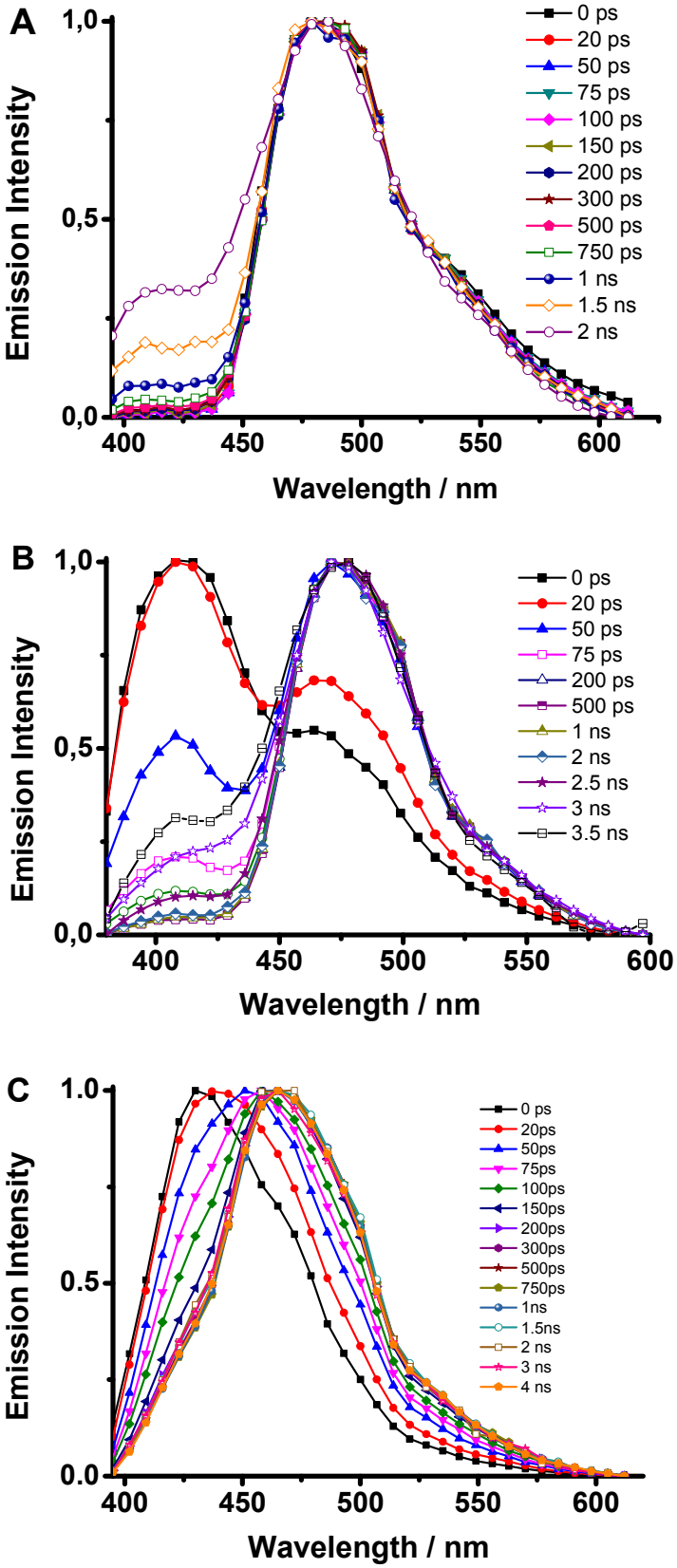

Figure 4.

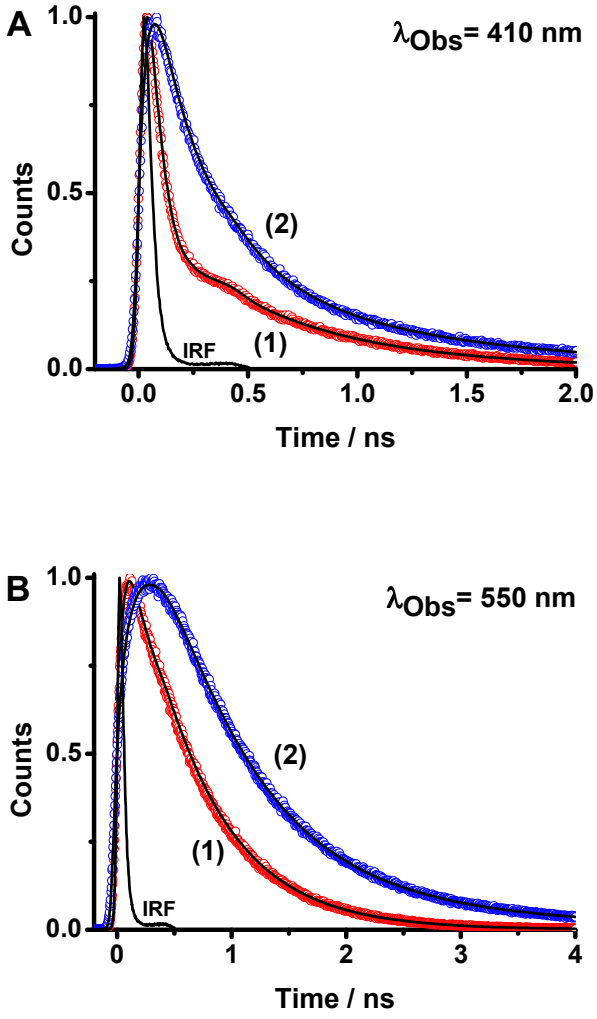

Figure 5.

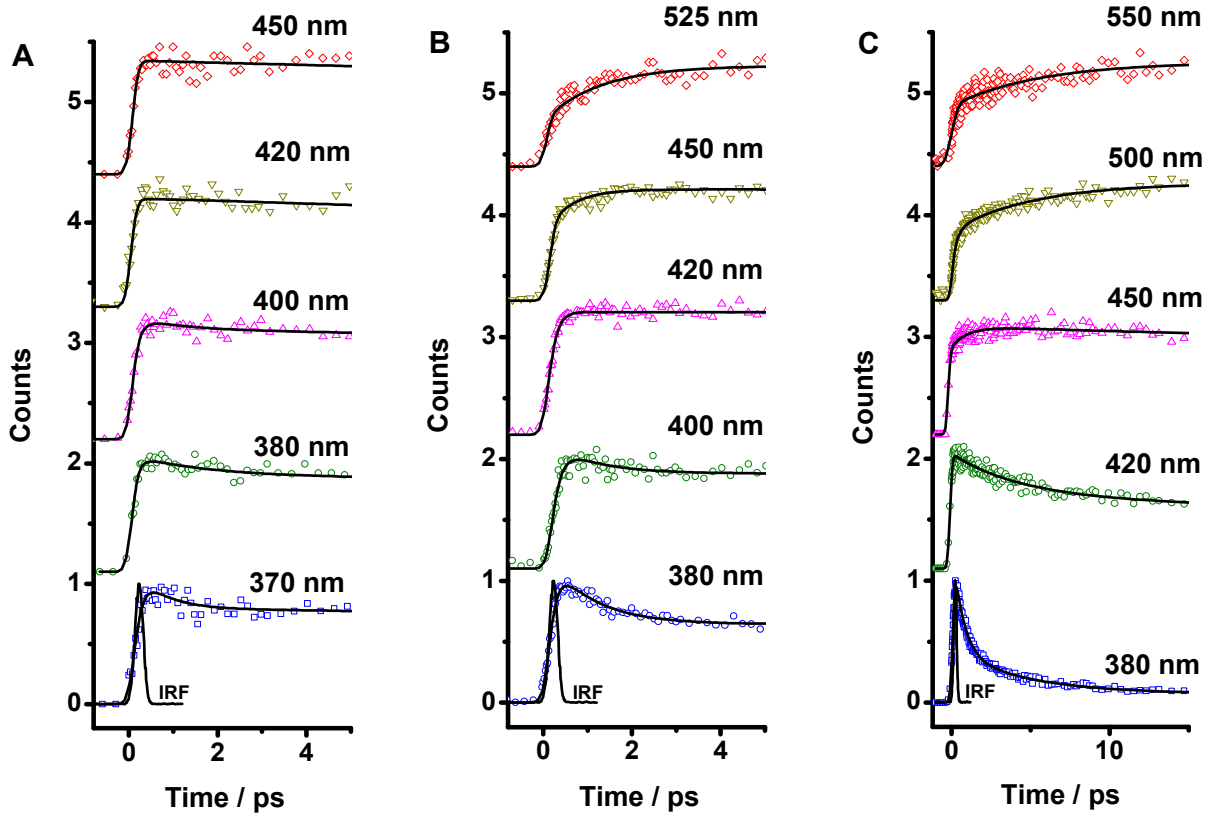

Figure 6.

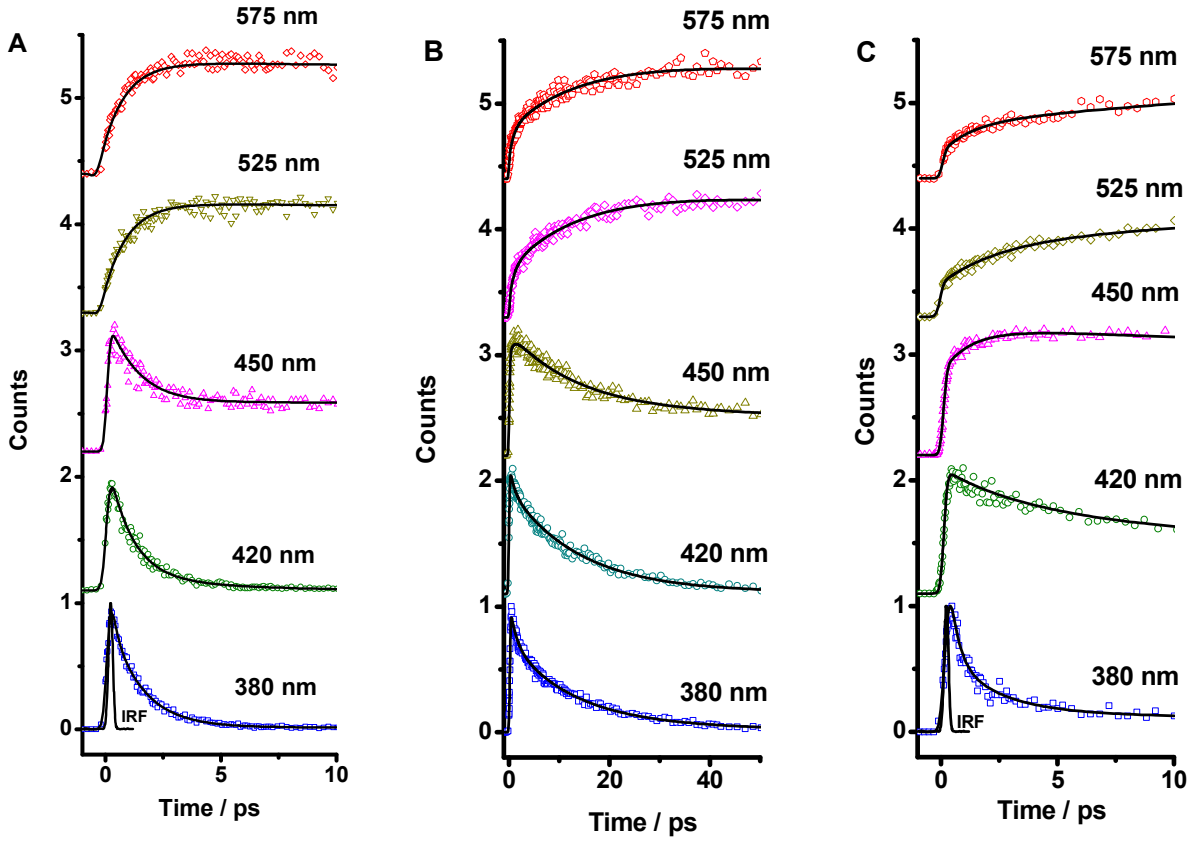

Figure 7.

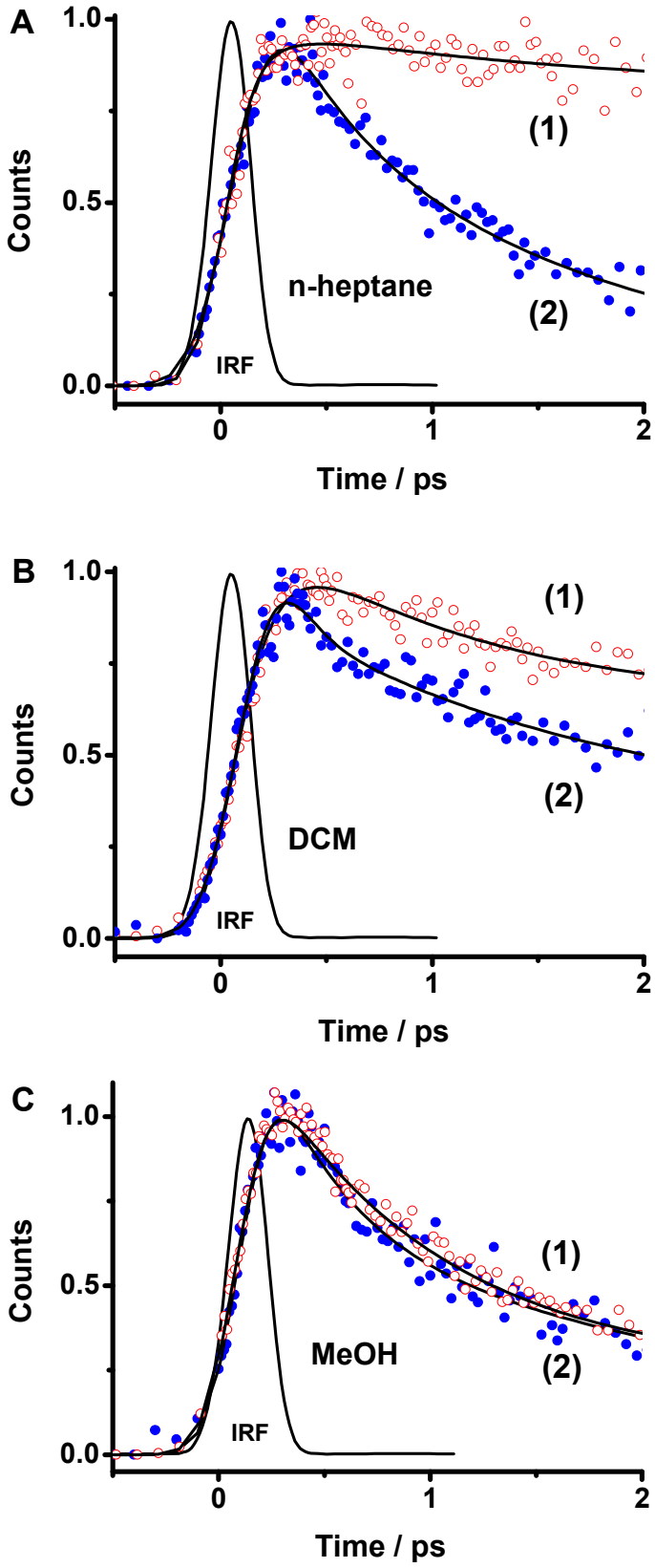

Table 1.

Molecule	Solvent	λ_{abs} nm	λ_{emis} nm	$\Delta\nu_{ss}$ cm^{-1}	FWHM cm^{-1}	φ_{CT}	φ_{K}	$k_{nr(CT)}$ / 10^8 s^{-1}	$k_{nr(K)}$ / 10^9 s^{-1}
	n-Heptane	327	385	4610	3740	0.52	-	2.7	-
6A-MBO	**DCM**	330	415	6025	3830	0.65	-	1.5	-
	MeOH	334	450	7900	3760	0.74	-	1.0	-
	n-Heptane	336	500	9630	3510	<0.001	0.04	-	2.3
6A-HBO	**DCM**	339	485	8710	3360	0.005	0.055	4.3	1.6
	MeOH	341	470	8180	3850	0.03	0.08	3.4	1.5

Table 2.

Solvent	λ_{Obs}/nm	τ_1 / ps	a_1	c_1	τ_2 / ps	a_2	c_2	τ_3 / ns	a_3	c_3
n-Heptane	395	-	-	-	420	75	46	1.5	25	54
	475	-	-	-	420	98	94	1.5	2	6
	500	-	-	-	420	100	100	-	-	-
	550	-	-	-	420	100	100	-	-	-
DCM	395	14	98	63	600	1	21	1.7	1	16
	430	14	76	9	600	23	85	1.7	1	6
	450	14	58	4	600	42	96	-	-	-
	475	14	(-)100	(-)100	600	100	100	-	-	-
	550	14	(-)100	(-)100	600	100	100	-	-	-
MeOH	395	35	85	24	615	15	76	-	-	-
	475	35	32	3	615	68	97	-	-	-
	500	35	(-)100	(-)100	615	100	100	-	-	-
	550	35	(-)100	(-)100	615	100	100	-	-	-
CD_3OD	410	200	71	30	780	23	38	2.4	6	32
	450	200	45	15	780	50	66	2.4	5	19
	475	200	(-)100	(-)100	780	95	86	2.4	5	14
	550	200	(-)100	(-)100	780	97	90	2.4	3	10

Table 3.

Solvent	λ_{Obs}/nm	τ_1 / fs	a_1	τ_2 / ps	a_2	τ_3* / ns	a_3
n-Heptane	380	140	-100	1.0	17	1.65	83
	420	140	-100	-	-	1.65	100
	450	-	-	-	-	1.65	100
DCM	380	140	-100	1.0	48	2.3	52
	420	160	-90	1.0	-10	2.3	100
	450	-	-	1.0	-100	2.3	100
	525	-	-	1.1	-100	2.3	100
MeOH	370	280	39	2.0	49	2.9	12
	380	280	35	2.0	43	2.9	22
	420	-	-	0.6	-100	2.9	100
	450	-	-	3.6	-100	2.9	100
	550	-	-	5.5	-100	2.9	100

Table 4.

Solvent	λ_{Obs}/nm	τ_1 / fs	a_1	τ_2 / ps	a_2	τ_3 / ps	a_3	τ_4* / ps	a_4
n-Heptane	395	140	-100	1.2	99	-	-	600*	1
	420	140	-100	1.2	98	-	-	600*	2
	450	-	-	1.2	62	-	-	600*	38
	475	-	-	1.1	-100	-	-	420	100
	600	-	-	1.2	-100	-	-	420	100
DCM	395	140	-100	1.0	31	14	67	600	2
	420	140	-93	0.9	-7	14	96	600	4
	450	-	-	1.0	-100	14	65	600	35
	475	-	-	1.1	-56	14	-44	600	100
	600	-	-	1.2	-20	14	-80	600	100
MeOH	380	250	55	2.1	38	35	10	615	2
	400	-	-	2.1	47	35	47	615	6
	430	-	-	0.8	-100	35	70	615	30
	475	-	-	2.0	-70	8.6	-30	615	100
	600	-	-	2.1	-15	35	-85	615	100

*Value obtained from a combination of the two components observed in TCSPC measurements.

Text for the TOC:

Stepwise and coupled photoinduced ICT and ESIPT reactions in a simple derivative of HBO in solution.